Modelling and bifurcation analysis of spatiotemporal hormetic effects on pest control

Liwen Song[a], Sanyi Tang[a], Changcheng Xiang[b], Robert A. Cheke[c], Sha He[a,*]

[a]School of Mathematics and Statistics, Shaanxi Normal University, Xi'an 710119, PR China
[b]School of Mathematics and Statistics, Hubei Minzu University, Enshi 445000, PR China
[c]Natural Resources Institute, University of Greenwich at Medway, Central Avenue, Chatham Maritime, Chatham, Kent, ME4 4TB, UK

Abstract

A discrete hormetic Ricker model (HRM) of a population with instant pulse perturbation between two consecutive generations can generate hormetic effects. For example, analysis of complex three-parameter spaces with the intrinsic growth rate, intervention strength, and dose timing as parameters revealed hormetic biphasic dose and dose timing responses. These responses exhibited either a J-shaped or an inverted U-shaped pattern, yielding a homeostatic change or a catastrophic shift and hormetic effects in many parameter regions. However, whether it is pest control or the effectiveness of treatments of tumors with radiotherapy and/or chemotherapy, the phenomenon is linked to the size of the space in which the parameters are located. Thus, the occurrence of hormetic effects is associated with spatiotemporal heterogeneity. To show this, we have developed an integro-difference equation based on the HRM that can describe the complex dynamics and hormetic effects in pest populations in two-dimensional space. Our findings indicate that factors such as the spatial domain, spatial grid, the dosage, and timing of control applications, and the intrinsic growth rate of the pest can significantly affect the spatial and temporal characteristics of pest populations and diverse biological phenomena in two-dimensional space. In particular, under the same size of spatial domains (or the same number of spatial grids), the smaller the spatial grids (or the larger the spatial domain), the stronger the hormetic effects of low dose stimulation and high dose inhibition will be. These factors include larger maximum responses and higher toxic thresholds. Therefore, optimal pest control measures should not only rely on the efficiency of a pesticide and its application time but should also be based on the spatial domain and the designing of reasonable

*corresponding author: Sha He, E-mail address:hesha@snnu.edu.cn

grid-based control strategies to avoid hormetic effects.

Keywords: Hormetic effects; Integro-difference equation; Extended Ricker model; Spatial heterogeneity; Pest management

1. Introduction

Proper use of pesticides or integrated pest management measures can effectively curb the growth of pest populations and even eradicate them. However, it is known that incorrect use of pesticides may not control pests effectively and can also lead to rapid increases in the number of pests, thus inducing bigger outbreaks, so-called hormesis or hormetic effects [1–3]. The phenomenon of hormesis is apparent when exposure to high levels of stressors is inhibitory but low doses are stimulatory [4–6]. Hormesis not only has short-term practical impact on agricultural production but also affects the interactions between species and the ecological structure and function of agricultural ecosystems [7–9]. Similarly, the phenomenon also exists in the treatment of tumours. The correct design of individual-based tumour treatment schemes, combined with the use of synergistic effects such as radiotherapy, chemotherapy, and immunotherapy, can effectively inhibit the growth of tumour cells [10, 11]. However, if the doses of radiotherapy and chemotherapy, cytokines and effector cells are not used properly, they can also lead to a rapid increase in tumour cells rather than curb their growth [12–17].

Recently, hormetic effects have been found in many studies, providing significant challenges for decision-making in the management of tumours [18–21], various other diseases [22], nutrition [23] and in ecotoxicology [24]. Thus, how to avoid and apply hormetic effects has become the focus of attention and research in many fields. Strategic applications of hormetic effects have shown promise in optimizing the management of agro-ecological systems with pesticides [25, 26] and harvesting [27–29] in relation to variations in endogenous regulatory mechanisms, intervention timings and dose-response specifics. For example, repeated applications of pesticides have unexpected consequences due to Volterra's principle, when an application of pesticides in a predator-prey system that kills predator and prey in proportion to their population sizes increases the prey population [30].

There is a big gap separating experimental designs and field observations from mathematical models that can be parameterized by experimental data sets, and which also exhibit hormetic effects. Therefore, how to reveal the mechanism of hormetic effects and provide a decision-making basis for effectively

avoiding hormetic effects during pest control and tumour treatment is of considerable importance. To bridge the gap, we not only need to construct multiple factor interaction models that can depict both the natural growth of pest populations or tumour cells, but also model the impact of human interventions on them. Due to the relatively short implementation time of human intervention measures, compared to the time scale of pest population growth or tumour evolution, it can be assumed that the intervention measures occur instantaneously. Moreover, impulsive differential equations can provide a natural characterization of these pulsed interventions [31], such as periodically spraying pesticides to curb the growth of pest populations, and periodically using radiotherapy, chemotherapy, and immunotherapy to suppress the growth of tumour cells.

Based on a continuous growth Logistic model with observation intervals interrupted by an external dose at a particular time between the observations [32], Tang *et al.* derived a corresponding discrete hormetic Ricker model by employing the piecewise continuous method. The proposed model has three critical parameters: the intrinsic growth rate, the dose-response and the timing of dose interventions [33] as follows:

$$\begin{aligned} N_{n+1} &= pN_n \exp\left[r\left(1-\frac{N_n}{K}\right)\theta + r\left(1-\frac{pN_n}{K}\exp\left(r\left(1-\frac{N_n}{K}\right)\theta\right)\right)(1-\theta)\right] \\ &= pN_n \exp\left[r\left(1-\frac{N_n}{K}\left(\theta+(1-\theta)p\exp\left(r\left(1-\frac{N_n}{K}\right)\theta\right)\right)\right)\right], \end{aligned} \tag{1.1}$$

where N_n is the population density of pests (or tumour cells) in generation n, r is the intrinsic growth rate and K denotes the carrying capacity, the parameter $p = 1-q$ denotes the survival rate after the pesticide has been sprayed at $n+\theta$ within each generation.

The interesting results obtained in [34] revealed through equilibrium stability conditions and bifurcation analyses that these three parameters completely determine the dynamic behaviour of the hormetic Ricker model (HRM), and determine the parameter spaces and occurrences of hormetic effects. If the lag factor is taken into account in HRM, it is generalized to an HRM model with time delays [32], and the main results proposed in [34] show that the HRM with time delay is universal and can fit U-shaped or inverted U-shaped data sets obtained in many different experiments and fields.

However, due to the obvious spatial heterogeneity involved in pesticide spraying, the factors that determine the success or failure of pest control not only depend on the growth rate of the pest itself, but

also depend on the spatial area where the pest population grows. In particular, the size of the spatial area determines the spread range of individual pests and even the spread speed. Similarly, the design of strategies such as radiotherapy and chemotherapy for tumours has also been related to the size of the tumour, especially the spread rate of tumour cells. Therefore, how to consider spatial factors in the HRM model and address the impact of spatiotemporal heterogeneity on the occurrence of hormetic effects, especially the impact of spatial size on the complex parameter spaces in which hormetic effects occur, is the main issue to be considered in this paper.

Integro-difference equations are often used to describe the spatial and temporal characteristics of biological populations. In 2008, Li *et al.* [35–38] used the integro-difference equation to describe the growth and dispersal processes of single and multiple populations, and explored the spatial patterns of travelling wave solutions. They also considered a competition model in the case of two species invading a habitat consecutively [39]. Within the last two years, Liu and Zhang *et al.* [40–42] combined the integro-difference equation with infectious disease models to analyze the existence of travelling wave solutions for various types of models, and recently introduced the distribution time delay to describe the existence and non-existence of travelling wave solutions [43]. Liang *et al.* [44] analyzed the existence of travelling wave solutions of the system by constructing integro-difference equations, and the complex kinetic behaviour and hormetic effects of a single population of organisms were described numerically.

Therefore, based on the three parameter HRM, in the present paper we propose a two-dimensional spatial diffusion discrete HRM using the modelling idea of integro-difference equations, focusing on the effects of spatial domain, intrinsic growth rate, dose-response and dose timing response on the occurrence of hormetic effects. In Section 4, we investigate how these four parameters affect the dynamic characteristics and hormetic effects on pest populations in two-dimensional space. We also consider how the development of the pest population is affected when different concentrations of pesticides are sprayed at different locations, i.e. we focus on the influences of spatiotemporal heterogeneity, the intrinsic growth rate of the pest populations, the insecticide efficiency and insecticide application timings on the complex dynamics and the occurrence of hormetic effects. Finally, in Section 5, we summarize the significance and limitations of this study.

2. Modelling spatio-temporal hormetic effects

In order to address the effects of spatial-temporal factors on the hormesis, we propose a discrete pest population growth model with population dispersion described by an integro-difference equation based on the hormetic Ricker model (HRM) of Tang [34], in which a single impulsive chemical control tactic is implemented within each pest generation. To address this, we assume that the pest population has two stages in its life cycle: a growth stage and a dispersal stage. Moreover, pulse control measures including spraying pesticide are implemented during the growth stage, which have strong spatial and temporal heterogeneity, and the pest population cannot increase when it is in the dispersal stage. The order of these two steps (reproduction/dispersal or dispersal/reproduction) is not important mathematically, although it can have significant biological repercussions for a discussion in the context of plants [45]. As mentioned in the introduction, the main purpose of this paper is to address the effects of space and time on hormesis during pest control operations.

2.1. Pest growth model during the growth stage

Using a similar model deduction method as was used by Tang *et al.* [34] and considering the above spatiotemporal factors, we let $N_n(x,y)$ be the density of the pest population at position (x,y) (i.e., a fixed observation point) of generation n, and $n = 0, 1, 2, \cdots$.

Pest control such as spraying pesticide often occurs at a certain time θ between two generations of pest population growth and $\theta \in [0,1]$, i.e. the control measure occurs at time $n+\theta$. At the same time, a proportion of pests with a ratio of q is killed. Due to spatiotemporal heterogeneity of the spraying, the killing rate q depends on the spatial position (x,y), i.e. $q = q(x,y)$, and consequently the survival rate $p \triangleq p(x,y) = 1 - q(x,y)$ is also space-dependent. Thus, after spraying pesticides, the number of pests at time $n+\theta$ has been reduced to:

$$N_{\theta^+}(x,y) \doteq N_{n+\theta^+}(x,y) = p(x,y)N_{n+\theta}(x,y) \tag{2.1}$$

and the sign $+$ represents the time after the pesticide spraying. According to the HRM model proposed

by Tang *et al.* [34], we have the following model during the growth stage

$$N_{n+1}(x,y) = p(x,y)N_n(x,y)\exp\left[r\left(1-\frac{N_n(x,y)}{K}\left(\theta+(1-\theta)p\exp\left(r\left(1-\frac{N_n(x,y)}{K}\right)\theta\right)\right)\right)\right]. \tag{2.2}$$

Note that there are two special cases in model (2.2), i.e. when $\theta = 0$ and $\theta = 1$, when the model degenerates to

$$N_{n+1}(x,y) = p(x,y)N_n\exp\left[r\left(1-\frac{pN_n(x,y)}{K}\right)\right] \tag{2.3}$$

or

$$N_{n+1}(x,y) = p(x,y)N_n(x,y)\exp\left[r\left(1-\frac{N_n(x,y)}{K}\right)\right]. \tag{2.4}$$

The theoretical analysis and dynamic behaviour of the above two cases with spatial homogeneity have been extensively investigated [46–48]. If we denote that the stable spatial homogeneity fixed point with spatial homogeneity of model (2.2) is N^*, which can be determined by the following equation:

$$p\exp\left[r\left(1-\frac{N^*}{K}\left(\theta+(1-\theta)p\exp\left(r\left(1-\frac{N^*}{K}\right)\theta\right)\right)\right)\right] = 1 \tag{2.5}$$

and we denote the function $F(N^*)$ as follows

$$F(N^*) = p\exp\left[r\left(1-\frac{N^*}{K}\left(\theta+(1-\theta)p\exp\left(r\left(1-\frac{N^*}{K}\right)\theta\right)\right)\right)\right]-1 \tag{2.6}$$

and further let $F(N^*) = 0$, we can get

$$N_1^* = \frac{K}{r\theta}[1-W(0,A)], \quad N_2^* = \frac{K}{r\theta}[1-W(-1,A)],$$

where $A = \frac{\theta}{(\theta-1)p^{\theta}e^{-r}}$, and $W(\cdot,\cdot)$ indicates the Lambert W function, for which more concepts and properties are given in references[49, 50].

Under the condition of spatial homogeneity, the existence and stability of equilibria of model (1.1) have been addressed by Tang *et al.* [34], and the dynamics of the proposed model can be determined by three parameter (growth rate, dose-response and dose timing response) spaces. Theoretical analyses and numerical investigations showed that the model with three critical parameters exhibited hormetic biphasic

dose and dose timing responses, either in a J-shape or an inverted U-shape, yielding a homeostatic change or a catastrophic shift and hormetic effects in many parameter regions. Moreover, the main results can be confirmed by fitting the proposed model to both hormetic and non-hormetic data sets.

2.2. *Pest growth model in the dispersal stage*

We assume that the pest population can disperse from one location to others in the plane and that the total scope of the population is invariable in this stage. Thus letting

$$F(N_n(x,y)) = p(x,y)N_n \exp\left[r\left(1-\frac{N_n(x,y)}{K}\left(\theta+(1-\theta)p(x,y)\exp\left(r\left(1-\frac{N_n(x,y)}{K}\right)\theta\right)\right)\right)\right], \tag{2.7}$$

then it follows from model (2.2) that

$$N_{n+1}(x,y) = F\left(N_n(x,y)\right). \tag{2.8}$$

Taking spatial heterogeneity into account, the density of the pest population should depend on its position (x,y), i.e. $N_n(x,y)$ represents the density of the pest population of generation n at position (x,y). Therefore, it follows from previous research [51] that the growth and dispersal of the pest population can be modelled as follows:

$$N_{n+1}(x,y) = \int_{-\infty}^{+\infty}\int_{-\infty}^{+\infty} L(x,y)F\left(N_n(x,y)\right)dxdy. \tag{2.9}$$

The basic form of dispersals for any species will be a form of dispersal kernel derived from the heat equation (for random diffusion in a plane):

$$L(x,y,T) = \frac{1}{4\pi\mu T}\exp\left[-\frac{x^2+y^2}{4\mu T}\right], \tag{2.10}$$

where T represents the dispersal time of a species and μ is a species-specific parameter describing the 'diffusivity' or rate of dispersal. We assume that there are two distinct stages that define the life cycle of the modelled organism: a sedentary stage and a dispersal stage. All growth occurs during the sedentary stage and all movement occurs during the dispersal stage. These assumptions allow us to regard the

dispersal stage as the combination of a linear operator and a nonlinear operator for the sedentary stage [52]. Thus, the mathematical blueprint for the integro-difference model is organized as follows.

Step1: Calculate the number of pests based on the last population values:

$$\begin{aligned} N_n^+(x,y) &= F(N_n(x,y)) \\ &= pN_n(x,y)\exp\left[r\left(1-\frac{N_n(x,y)}{K}\left(\theta+(1-\theta)p\exp\left(r\left(1-\frac{N_n(x,y)}{K}\right)\theta\right)\right)\right)\right]. \end{aligned} \tag{2.11}$$

Step2: Disperse the population using convolutions as described above:

$$N_{n+1}(x,y) = \int_{-\infty}^{+\infty}\int_{-\infty}^{+\infty} L(x,y) * N_n^+(x,y)dxdy. \tag{2.12}$$

Based on the above two steps, we can numerically deduce the future population level from the current population level in the following way:

$$\begin{aligned} N_{n+1}(x,y) &= \int_{-\infty}^{+\infty}\int_{-\infty}^{+\infty} L(x,y)F(N_n(x,y))\,dxdy \\ &= \int_{-\infty}^{+\infty}\int_{-\infty}^{+\infty} \frac{1}{4\pi\mu T}\exp\left[-\frac{x^2+y^2}{4\mu T}\right] p(x,y)N_n(x,y) \\ &\quad \exp\left[r\left(1-\frac{N_n(x,y)}{K}\left(\theta+(1-\theta)p(x,y)\exp\left(r\left(1-\frac{N_n(x,y)}{K}\right)\theta\right)\right)\right)\right] dxdy. \end{aligned} \tag{2.13}$$

3. Bifurcation analyses without spatial diffusion

The analysis of the full model (2.1) with spatial diffusion and heterogeneity is quite challenging. This section begins with the analysis of the model without spatial diffusion, i.e., assuming that $p(x,y)$ is a constant p. We study the dynamic behavior of the model, including flip bifurcation and chaotic dynamics. In the next section, we primarily explore the spatial influence through numerical simulations.

3.1. Flip Bifurcation

As mentioned in the previous section, there are two non-zero fixed points of the model (2.1). According to Lemma 2 in the supplementary material of reference [34], the model (2.1) has a positive fixed point $E^* = N^*$ if $pe^r > 1$. After a simple analysis, there exists an eigenvalue $\lambda = -1$ if the following

conditions holds

$$C(N^*) = B_2B_3(rpB_1B_4N^* + K)p + K^2 = 0, \tag{3.1}$$

where $B_1 = e^{\frac{r(K-N^*)a}{K}}$, $B_2 = e^{\frac{(B_1)a-1)p-a)N^*+K)r}{K}}$, $B_3 = K - \theta N^* r$ and $B_4 = \theta - 1$.

Theorem 3.1. *For system (1.1), if $pe^r > 1$ and $C(N^*) = 0$, a flip bifurcation occurs at the fixed point $E^* = N^*$.*

Proof. The proof for flip bifurcation can be found in the Appendix A.

□

3.2. Chaotic dynamics

The value of the Lyapunov exponent is considered to be one of the characteristics implying the existence of chaos [53, 54]. The calculation of the Lyapunov exponent is performed in the Appendix B.

To further illustrate the chaotic dynamics for model (1.1), we choose the parameters q and θ as the bifurcation parameter and fix all other parameters. The maximum Lyapunov exponent Λ is calculated and the bifurcation diagrams are plotted in Fig. 1. As shown in Fig. 1, the maximum Lyapunov exponent Λ may be larger or less than 0 as parameters q and θ vary. Correspondingly, the trajectory tends to a chaotic solution when $\Lambda > 0$; the trajectory tends to a fixed point or periodic solution when $\Lambda < 0$. For example, we observe that the system is stable for $q \in [0.489, 1]$ in Fig. 1(a), and the periodic solution changes from 4 to 2, and at 1 becomes the solution of period 1. The maximum Lyapunov exponents are positive, indicating the existence of chaotic attractors when $q \in [0, 0.488]$. We can see that there exists a stable interval for $\theta \in [0.081, 0.887]$ from Fig. 1(b), meanwhile a pseudo-periodic solution appears. It is worth mentioning that we can also see from Fig. 1 that there are flip bifurcation phenomena.

When considering spatial diffusion, the population density changes follow model (2.13). For such a one-dimensional integral difference equation, there has not been any theoretical research on a bifurcation analysis of it so far, so we are unable to conduct such an analysis. Instead, we will explore the dynamics of model (2.13) using the numerical simulation results. Our purpose is to address how spatial heterogeneity affects the hormetic effects and determines the parameter spaces. In the next section, we present the bifurcation diagrams for system (2.13) to confirm that model (2.13) inherits the dynamical

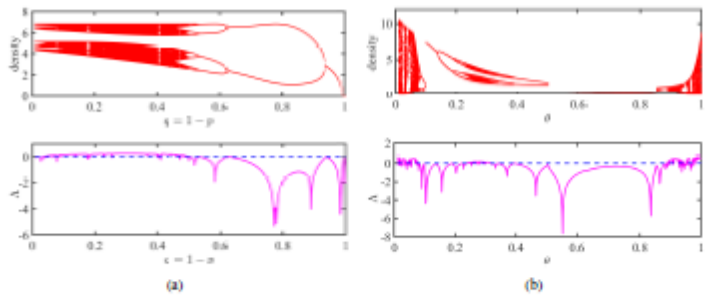

Figure 1: Bifurcation diagrams and maximum Lyapunov exponent Λ with q and θ covering [0, 1]. (a) $\theta = 0.15, r = 5.18$, (b) $q = 0.2, r = 5$. The other parameters are fixed as follows: $N(0) = 0.35, K = 1$.

behavior that model (1.1) possesses and to show the new interesting complex dynamical behavior by using numerical simulations.

4. Spatiotemporal hormetic effects and bifurcation analyses

Note that it is theoretically difficult to study and analyse the existence of plane waves and the corresponding solutions of model (2.13) in two-dimensional space due to the complexity of function $F(N_n(x,y))$, so we choose an alternative way to reveal the influences of the space dependent control measures on the hormetic effects during the pest growth stage. To do this, we need to solve the integro-difference equation (2.13) numerically. Thus, without loss of generality we assume that the space is a square region with length ls and the number of grids sd in the two-dimensional plane, and we will use the Dirichlet boundary condition to treat the boundaries of the space, assuming that the number of pests at the boundary is reduced to half at the end of the current generation.

We will reveal the influences of spatial domain ls and its spatial grid sd, the intrinsic growth rate r and the factors related to the control measures including the killing rate q (a parameter related to the pesticide dose) and the time of spraying insecticide θ on the dynamics and hormetic effects. Moreover, we also focus on the effects of spatial homogeneity and heterogeneity of control measures on the hormesis, i.e. the killing rate q is a constant or it depends on the space position (x,y), which allows us to design the space-based optimal prevention and control strategy.

4.1. The dynamic complexity and hormetic effects under the constant killing rate q

4.1.1. The solutions of the model (2.13) with some key parameters change

We first address the effects of spatial homogeneity of control measures on the dynamics. Let the instant killing rate $q(x,y) = q$ be a constant that does not depend the spatial position (x,y). Throughout the paper we denote the intermediate location $x/2$ (or $y/2$) as x^* (or y^*). If we fix the parameter set as in Fig. 2, we can get the three types of classical solutions of $N_n(x,y)$ over 100 generations at a fixed observation position $(x^*,y(:))$ of model (2.13): the spatial homogeneous equilibrium (Fig. 2(a)); the spatial heterogeneous periodic solution with a period of 4 (Fig. 2(b)); and spatial heterogeneous chaotic solutions (Fig. 2(c)), as shown in the first column of Fig. 2.

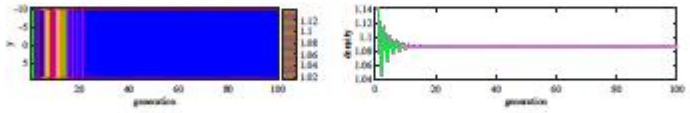

(a) $r = 4, q = 0.3, \theta = 0.72$

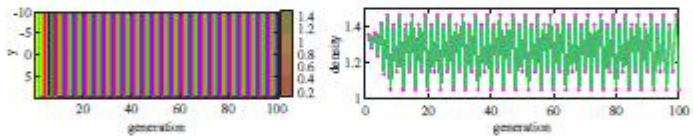

(b) $r = 5.5, q = 0.2, \theta = 0.66$

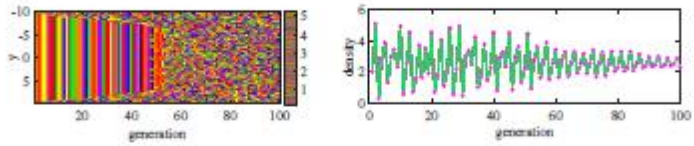

(c) $r = 5.5, q = 0.2, \theta = 0.3$

Figure 2: The left column shows three types of classical solutions of $N_n(x,y)$ over 100 generations at a fixed observation position $(x^*,y(:))$ of model (2.13), and the right column is the spatial average solution curves of the three typical solutions shown in the left column with respect to the spatial variable y. The other parameters are fixed as follows: $nd = 128, D = 20, K = 1, \mu = 0.02, T = 0.1$.

In order to more clearly show the effects of spatial locations on the solutions, we intuitively reveal the impact of spatial location on different types of solutions through numerical investigations in Fig. 2. Therefore, we fix the spatial location x^*, and focus on the changes in the solutions in the y space and the changes in the solution curves averaged over the y space. The left column shows the spatial distribution of population density at spatial location $(x^*, y(:))$, and the right column is the spatial average solution curves of three typical solutions shown in the left column with respect to the spatial variable y.

In particular, Fig. 2(a) with fixed parameters $(r = 4, q = 0.3, \theta = 0.72)$ reveals that the pest population eventually stabilises at the spatial homogeneous equilibrium (i.e. $N_*(x, y) = 1.09$). In this case, due to the homogeneity of population distribution, spatially consistent pest control strategies can be adopted to achieve unified control objectives without incurring hormetic effects. The periodic solution with uniform spatial distribution and time period is provided in Fig. 2(b) with parameters $r = 5.5, q = 0.2, \theta = 0.66$, this indicates that it is very important to monitor the population size of generations and design prevention and control strategies based on the dynamic changes of the population size of generations. In Fig. 2(c), we set the parameter values as $r = 5.5, q = 0.2, \theta = 0.3$, and this type of solution not only presents chaotic time series, but also has strong heterogeneity in spatial distribution. Therefore, it is necessary to design space-time based prevention and control measures to reduce the parameter spaces where hormetic effects occur.

4.1.2. The occurrence of hormetic effects under different spatial grid

We first focus on how the spatial grid sd affects the solution $N_n(x, y)$ of the model (2.13), and consequently on the hormetic effects. Here we fix $r = 1.9$ and $ls = 20$ for different spatial grids to explore how the factors related to the control measures affect the evolution of pest populations. Time average steady-state solutions $N(x^*, y^*)$ of model (2.13) over the last 50-100 generations at a fixed observation point (x^*, y^*) for different q and θ values are shown in Fig. 3(a)-Fig. 3(c). Fig. 3 clearly demonstrates the effects of spatial grid sd, insecticide dose q and time θ on the dynamical behaviour and hormetic effects of populations, where (x^*, y^*) represents the central point of the two-dimensional space.

From Fig. 3(a), we can see that when the spatial grid sd is 32, the pest population increases sharply and then decreases as the application time θ increases. When the spatial grid sd is relatively large (see Fig. 3(b) and Fig. 3(c)), the evolution of the population exhibits an inverted U-shape (occurrence of

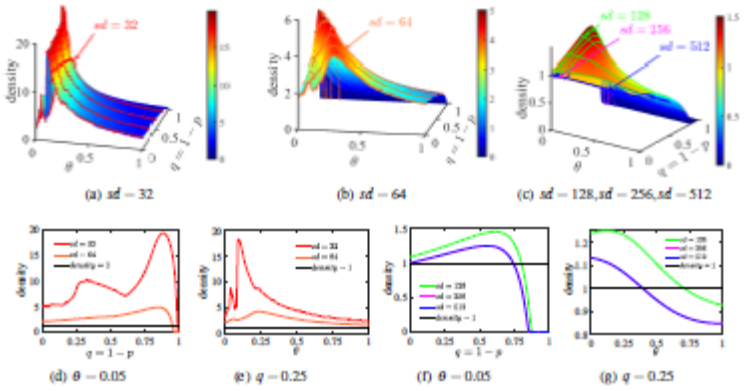

(a) $sd = 32$ (b) $sd = 64$ (c) $sd = 128, sd = 256, sd = 512$

(d) $\theta = 0.05$ (e) $q = 0.25$ (f) $\theta = 0.05$ (g) $q = 0.25$

Figure 3: Hormetic effects for spatial grid. The steady-state solutions $N(x^*, y^*)$ at a fixed observation point (x^*, y^*) and time-average over the last 50-100 generations for different q and θ values. The other parameters are fixed as follows: $r = 1.9, Is = 20, K = 1, \mu = 0.02, T = 0.1$.

hormetic effects) as the killing rate q increases, i.e. the regenerative capacity could be enhanced if a low dose of pesticide is applied, and inhibited inversely if the concentration of pesticide exceeds a threshold. Note that the smaller the spatial grid sd, the more insecticide q is required for keeping the population within a certain level, as shown in Fig. 3(d) and Fig. 3(f). However, when the insecticide q exceeds a certain threshold such as a toxic threshold, the population density approaches 0, in which case the population becomes extinct.

The spatial surfaces shown in Fig. 3(c) and curves shown in Fig. 3(f) and Fig. 3(g) almost coincide when the spatial grid sd is large enough ($sd = 256$ or $sd = 512$). It indicates that the changes in the grid have very little impact on the stable population levels, hormetic effects. As shown in Fig. 3(d)-Fig. 3(g), it is interesting that increases in the size of the spatial grid can significantly reduce the toxic threshold. In addition, not only can the dosage of pesticide induce low dose stimulation and high dose inhibition, but different usage times at fixed doses can also cause hormetic effects (see the intersection of the black line (the density of pest is equals to 1) and other coloured line). Moreover, we can see that the stronger the intensity of population growth stimulated by low doses with a multiple inverted U-shape curve (as shown in Fig. 3(d) and Fig. 3(e)) and J-shape curve (as shown in Fig. 3(f)).

The occurrence of hormetic effects and their parameter spaces strictly depend on the spatial grid, which indicates that spatially dependent control measures should be designed. For a given space size (i.e. $ls = 20$ here), the fewer spatial grids that there are, the larger the parameter space for the occurrence of hormetic effects. Specifically, prevention and control strategies implemented based on segmented spatial areas can effectively avoid the occurrence of hormetic effects, which is beneficial for pest control.

4.1.3. Bifurcation analysis under different spatial grid

In order to reveal the impact of spatial grid on the dynamic behaviour of the model (2.13), especially the mechanisms of occurrence of hormetic effects, we draw one-parameter bifurcation diagrams of the killing rate q, the intrinsic growth rate r and the dosage time response θ as shown in Fig. 4 - Fig. 6, respectively. From Fig. 4(a) and Fig. 4(b), we can see that the density increased firstly and then decrease as q increase when the spatial grid $sd = 256$ and $sd = 128$. They present one common features of hormesis: hormetic biphasic dose-responses (inverted U-shape) of low dose stimulation and high-dose inhibition. A large stable fixed point is generated under low dose stimulation, which reveals the homeostatic changes caused by external stimulation. The piecewise continuous inverted U-shape curves demonstrate the significance of catastrophic shifts [12] and the robustness of the stability induced by external stimulations in homeostatic alterations in producing a hormetic-like biphasic dose-response curve[55]. From Fig. 4(c), the flip bifurcation and chaotic phenomenon occurs when the spatial grid $sd = 64$. By comparing the bifurcation diagrams of the parameter q with different values of sd, we can find that the smaller the sd, the greater the density of the population, which means that the regeneration ability of the system is further enhanced, resulting in the more obvious hormetic effects. In addition, the system become more stable with the spatial grid increase. Thus, we can design effective prevention and control strategies while avoiding the occurrence of hormetic effects based on a reasonable grid segmentation.

In order to reveal how the intrinsic growth rate r affects the dynamic behavior of the population, we draw a bifurcation diagram shown in Fig. 5. It can be seen from Fig. 5 that when the intrinsic growth rate r increases, not only does it increase the complex dynamic behaviour of the system, but it also significantly increases the likelihood of the system experiencing low-dose stimulation and high-dose inhibition, revealing two mechanisms of hormetic effects: homeostatic change and catastrophic shift. It is worth noting that the pest population transitioning from the monostable state or coexisting

bistable/multistable states to chaos with respect to r. We can see that there exists a threshold r that causes the system to transition from a stable state to an another stable state (see Fig. 5(a) and Fig. 5(b)). The dosage time response θ may also be closely related to the hormetic effects. In Fig. 6, we fix $q = 0.2$, a slight change in θ can cause the system to transition from one stable state to another stable or unstable state with a larger peak. The low level of stimulation reduces the competition within the population, improves the regeneration ability of the population, and makes population density exceed the original environmental carrying capacity.

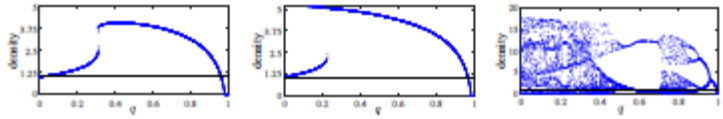

(a) $sd = 256$ (b) $sd = 128$ (c) $sd = 64$

Figure 4: Bifurcation diagrams of parameter q with different sd at a fixed observation point (x^*, y^*) over 100 generations. The other parameters are fixed as follows: $ls = 20, \theta = 0.15, r = 4.5, K = 1, \mu = 0.02, T = 0.1$.

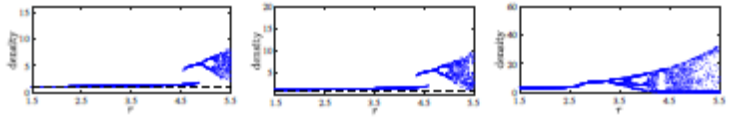

(a) $sd = 256$ (b) $sd = 128$ (c) $sd = 64$

Figure 5: Bifurcation diagrams of parameter r with different sd at a fixed observation point (x^*, y^*) over 100 generations. The other parameters are fixed as follows: $ls = 20, q = 0.2, \theta = 0.15, K = 1, \mu = 0.02, T = 0.1$.

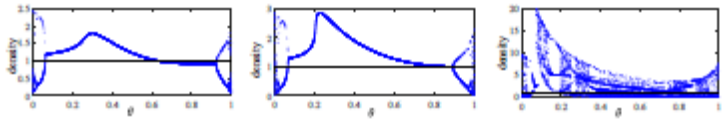

(a) $sd = 256$ (b) $sd = 128$ (c) $sd = 64$

Figure 6: Bifurcation diagrams of parameter θ with different sd at a fixed observation point (x^*, y^*) over 100 generations. The other parameters are fixed as follows: $ls = 20, q = 0.2, r = 4, K = 1, \mu = 0.02, T = 0.1$.

4.1.4. Dynamic complexicity revealed by Lyapnunov exponent under different spatial grid

In this section, we choose the key parameters (q, r, θ) to explore the chaotic dynamics of the system, and calculate the (q,r) and (θ,r)-dependence two-parameter Lyapunov exponents with the different values of sd. The occurrence of chaos when the Lyapunov exponents Λ larger than 0. In Fig. 7, we fix the value of parameter θ, and q and r are changing. In Fig. 7(a), it can be seen from the color distribution of the (q,r) parameter plane that the system is stable($\Lambda < 0$) in most parameter areas, while the emergence of chaos ($\Lambda > 0$) in only small area when the value of sd is 256. The distribution of the (q,r) parameter plane when the value of sd is 128 and 64 are shown in Fig. 7(b) and Fig. 7(c). We can see that the size of the parameter region where chaos occurs increases as sd decreases. This indicates that the smaller spatial grid sd, the less stable the system will be. However, when the value of q is fixed as 0.2, we change the parameter θ and r (see Fig. 8). The (θ,r) parameter plane exhibits a more widespread and intense chaos phenomenon. Similarly, we find that the size of the parameter region in which chaos occurs is larger as sd decreases, which means that a sufficiently large spatial grid sd needs to be set to ensure that pests do not break out.

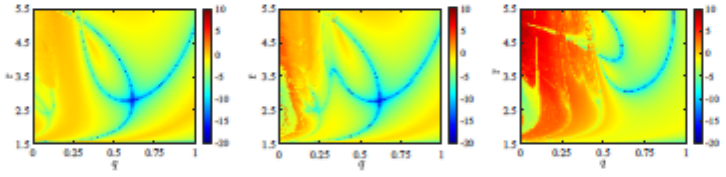

(a) $sd = 256$ (b) $sd = 128$ (c) $sd = 64$

Figure 7: (q,r)-dependence of the maximum Lyapunov exponent Λ with the different values of sd at a fixed observation point (x^*, y^*) and time-averaged over 100 generations. The other parameters are fixed as follows: $ls = 20, \theta = 0.15, K = 1, \mu = 0.02, T = 0.1$

4.1.5. The effect of spatial domain on the dynamic and hormetic effects

We addressed the effects of the spatial grid sd on the evolution of pest populations and hormesis in the Section 4.1.2-Section 4.1.4, and in this section we focus on the effects of the spatial domain ls. To do this, we fix the spatial grid as $sd = 256$ and explore how the different space domain ls influence the occurrence of hormetic effects. Similarly, we choose the killing rate q and dose time θ as the key parameters, and

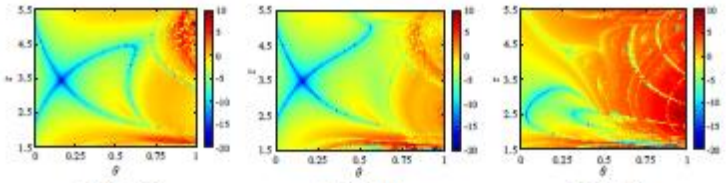

(a) $sd = 256$ (b) $sd = 128$ (c) $sd = 64$

Figure 8: (θ, r)-dependence of the maximum Lyapunov exponent Λ with the different values of sd at a fixed observation point (x^*, y^*) and time-averaged over 100 generations. The other parameters are fixed as follows: $ls = 20, q = 0.2, K = 1, \mu = 0.02, T = 0.1$.

plot the solutions of $N(x^*, y^*)$ of model (2.13) at a fixed observation point (x^*, y^*) and time-averaged over 50-100 generations for different ls, as shown in Fig. 9(a). The curves shown in Fig. 9(b) reveal that under the same number of spatial grids, the larger the spatial area, the more obvious of hormetic effects of low dose stimulation and high dose inhibition, including larger maximum responses and larger toxic thresholds. All these results indicate that if the spatial grid ls of the pest's habitat is larger, the pest is more likely to survive. This will result in a number of pest population increases, and the population regeneration ability will be improved, such that the pest population breaks out of its original low steady state and transfers to a higher stable (or unstable) state. Similarly, the dose time θ can generate the same effects for a given spatial domain, i.e. the larger the domain, the stronger the hormetic effects will be, as shown in Fig. 9(c).

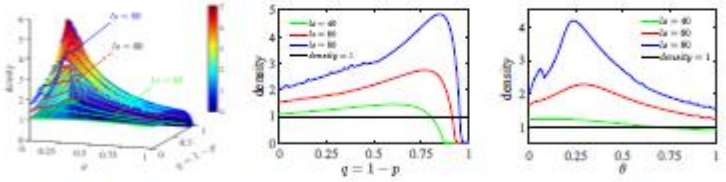

(a) $lx = 80, ls = 60, lx = 40$ (b) $\theta = 0.05$ (c) $q = 0.25$

Figure 9: Hormetic effects for different spatial domains. The steady-state solutions of $N(x^*, y^*)$ at a fixed observation point (x^*, y^*) and time-averaged over 50-100 generations for different ls values. The other parameters are fixed as follows: $sd = 256, r = 1.9, K = 1, \mu = 0.02, T = 0.1$.

Fig. 10 and Fig. 11 further reveal the spatial heterogeneity of hormetic effects, by showing how the

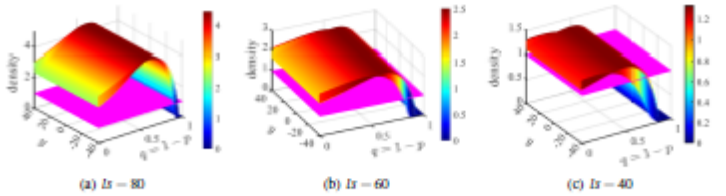

(a) $ls = 80$ (b) $ls = 60$ (c) $ls = 40$

Figure 10: The steady-state solutions at a fixed observation position $(x^*, y(:))$ with respect to q and time-averaged over 100 generations for different ls values. The other parameters are fixed as follows: $sd = 256, \theta = 0.15, r = 1.9, K = 1, \mu = 0.02, T = 0.1$.

spatial hormesis of the population are affected by the spatial domain ls, the killing rate q and dose time θ, respectively, where the pink plane represents the cross-section of $N_n(x, y) = 1$. It follows from Fig. 10 that with the change of $ls = 40$ to $ls = 80$ (the spatial domain increases), the hormetic effect of the population in the space is more intense, and the region of the hormetic effects is larger, at this time the system transitions from a stable state to an another stable state. In the case of fixed spatial domain ls, the population density showed a trend of low dose stimulation and high dose inhibition. It is clear from Fig. 11 that at a fixed the killing rate $q = 0.2$, the pest population density increases with the increase of spatial domain, and the density of the population will also increase first and then decrease or monotonicaly decreasing with the increase of θ with fixed spatial domain ls. Another interesting phenomenon is that in Fig. 10 and Fig. 11, it is obvious that the Dirichlet boundary condition is used to deal with the boundary, which means that what makes the population develop at the boundary is different from its causation at other positions.

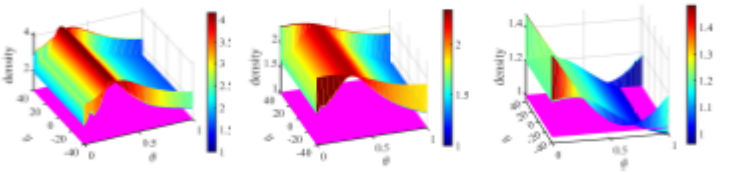

(a) $ls = 80$ (b) $ls = 60$ (c) $ls = 40$

Figure 11: The steady-state solutions at a fixed observation position $(x^*, y(:))$ with respect to θ and time-averaged over 100 generations for different ls values. The other parameters are fixed as follows: $sd = 256, q = 0.2, K = 1, r = 1.9, \mu = 0.02, T = 0.1$.

4.1.6. Parameter space analysis of the occurrence of hormesis effects

From the Section 4.1.2 and Section 4.1.5, we know that the parameters q and θ can significantly affect the occurrence of the hormesis effects. To further explore the parameter region where the hormesis occurs, we draw two-parameter $q-\theta$ plane diagrams that mark whether the paradox effect occurs or not under different values of sd and ls. Firstly, we fix ls as 20 and let sd change in Fig. 12(a-c), and it can clearly see that as the spatial grid sd decreases, the size of the parameter region where the hormesis occurs also increases, which means that the lower the spatial heterogeneity, the stronger the regeneration ability of the pest population. The main reason is that the population switches from low steady states to high steady states, or the population explodes in a certain parameter space, and the population is more susceptible to environmental impacts including spatial grids. Secondly, we fix sd as 256 and let ls change in Fig. 13(a-c). It can be seen from Fig. 13 that as the spatial domain ls decreases, the proportion of pesticide induced hormetic region decreases significantly. All these results confirm that the optimal pest prevention and control measures not only rely on the efficiency of pesticide and its application time, but also depend on the spatial domain and a reasonable grid design. The parameter spaces associated with hormetic effects occurrence are helpful to design implementation of a multi-strategy integrated management of the pest population.

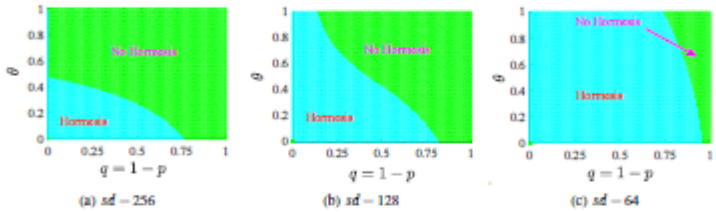

(a) $sd = 256$ (b) $sd = 128$ (c) $sd = 64$

Figure 12: (q,θ)-dependence of hormesis emergence with the different values of sd at a fixed observation point (x^*,y^*) and time-averaged over 100 generations. The other parameters are fixed as follows: $ls = 20, r = 1.9, K = 1, \mu = 0.02, T = 0.1$.

4.2. The dynamics and hormetic effects under the spatial dependent killing rate

Under the assumption of constant killing rate q, the above Section 4.1 systematically analyzed the influence of spatial grid and spatial domain on the dynamic behaviour of the model, especially on the

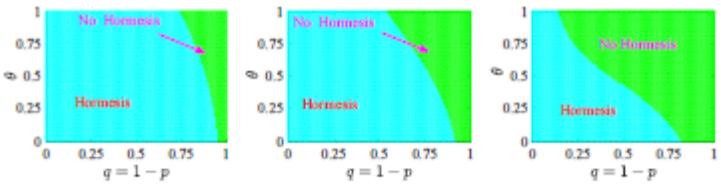

(a) $ls = 80$ (b) $ls = 60$ (c) $ls = 40$

Figure 13: (q,θ)-dependence of the hormesis emergence with different values of ls at a fixed observation point (x^*,y^*) and time-averaged over 100 generations, The other parameters are fixed as follows: $sd = 256, r = 1.9, K = 1, \mu = 0.02, T = 0.1$.

parameter space of occurrence of hormetic effects. The main conclusion reveals that the size of the space and the number of grids have a significant impact on it, and consequently it is very important to consider the killing rate function $q(x,y)$ as a function of space, i.e. spatial heterogeneity of pesticide efficiency. To do this, we assume that the $q(x,y)$ obeys a two-dimensional Gaussian distribution in two-dimensional space, so as to explore its influence on the spatial dynamics and hormetic effects on the pest population. Define the $q(x,y)$ as follows:

$$q(x,y) = \frac{e^{-(x^2+y^2)}}{ls \cdot 2^{0.05 \cdot ls}}, \tag{4.1}$$

where $x,y \in [-ls, ls]$.

The corresponding distribution of equation (4.1) in the two-dimensional space is shown in Fig. 14 with different spatial domains ls and spatial grids sd. Comparing each row with fixed $sd = 256$ in Fig. 14, it can be seen that as the spatial domain ls decreases, the number of pesticide sprays at the boundary is relatively small, and the change of pesticide concentration is relatively slow in the neighbourhood, which is also consistent with practical applications, and the spatial heterogeneity is enhanced. At the same time, in the case of the same spatial size ls, because of the different spatial grids sd, the concentration of sprayed pesticides will also be different in a certain neighbourhood range. The larger the spatial grid sd, the weaker the spatial heterogeneity, as shown in each column of Fig. 14.

Comparing the results shown in Fig. 2, it is clear that for the same parameter set fixed as in Fig. 15, the spatial heterogeneity of the populations is increased and the density of the population is relatively reduced for the three types of typical solutions. Note that on the spatial average the pest population eventually stabilises at the fixed point (i.e. $N_n(x,y) = 0.83$ which is less than the value in Fig. 2) when

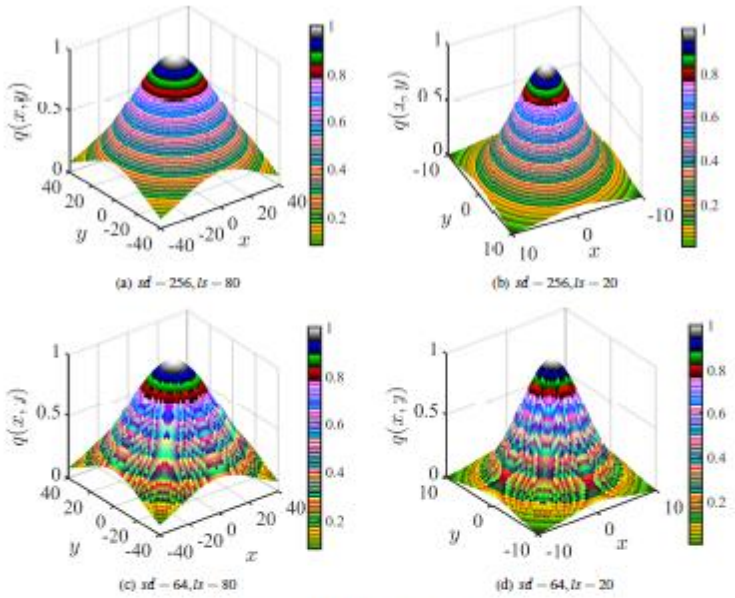

(a) $xd = 256, lx = 80$ (b) $xd = 256, lx = 20$

(c) $xd = 64, lx = 80$ (d) $xd = 64, lx = 20$

Figure 14: Gaussian distribution $q(x, y)$ for different spatial domains and spatial grids.

we fixed the parameter values as $r = 4, \theta = 0.72$ in Fig. 15(a). In Fig. 15(b) with fixed parameters $r = 5.5$ and $\theta = 0.66$, we note that the amplitude of the solution is relatively smaller than in Fig. 2(b), which indicates that the spatial dependent control measures are beneficial for pest control. Another interesting conclusion is that in the central region of space, the population size exhibits more regular changes, while in the adjacent boundary regions, it exhibits complex dynamic behaviour. Based on the definition of $q(x, y)$, the pesticide dosage in the middle area is high and this results in better and effective control effects, while the density of the pests on the border is complicated, with strong spatial heterogeneity due to low dosage, which could result in an increasing occurrence of hormetic effects at the border region.

Since the amount of pesticide sprayed depends on the spatial location (x, y), the spatial heterogeneity is enhanced, and there exist discrepancies between the densities of the pest population at different

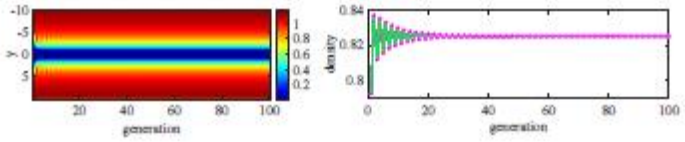

(a) $r = 4, \theta = 0.72$

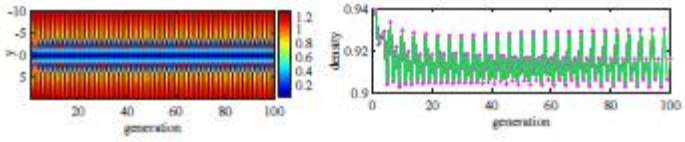

(b) $r = 5.5, \theta = 0.66$

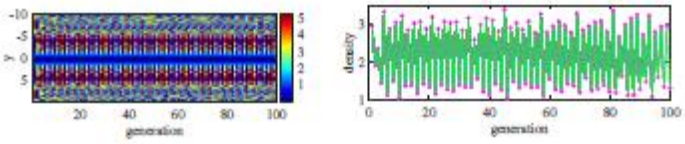

(c) $r = 5.5, \theta = 0.3$

Figure 15: The left column shows three types of classical solutions of $N_n(x, y)$ over 100 generations at a fixed observation position $(x^*, y(:))$, and the right column is the spatial average solution curves of three typical solutions shown in the left column with respect to the spatial variable y. The other parameters are fixed as follows: $sd = 128, ls = 20, K = 1, \mu = 0.02, T = 0.1$.

locations, which is not completely consistent with the phenomena described in Section 4.1.2 and Section 4.1.3, as shown in Fig. 16, where the pink plane represents the section of $N_n(x, y) = 1$. Fig. 16(a), Fig. 16(d) and Fig. 16(g) represent the spatial grid of $sd = 256, sd = 128, sd = 64$ respectively for the pest population at the spatial location $(x^*, y(:))$, (i.e. in the middle of the x direction) with respect to parameter θ. Fig. 16(b), Fig. 16(e), and Fig. 16(h) represent their curves at some given positions with respect to θ, and Fig. 16(c), Fig. 16(f), and Fig. 16(i) represent their curves at certain fixed times θ.

Under the condition of fixed spatial domain $ls = 20$ and $r = 1.9$, the pest population density presents symmetry about the central position, and differences also exist in different spatial positions, as shown

in Fig. 16. At the same location, as the dose time θ increases, the pest population also shows a pattern of increasing and then decreasing, and eventually stabilizes at a certain level, as shown in Fig. 16(b), Fig. 16(e) and Fig. 16(h). By comparing each row, we can see that as the spatial grid decreases, the final pest population density also increases. For a fixed θ, the concentration of pesticides in space follows a one-dimensional Gaussian distribution, $q(x^*, y)$ follows a pattern of increasing and then decreasing, as can be seen from Fig. 16(c), Fig. 16(f) and Fig. 16(i), where the pest population density also increases and then decreases.

Fig. 17 represents the variation in the pest population density at different positions in space with dose time θ under different spatial domains ls. In Fig. 17, we set the spatial grid to $sd = 256$, and we can see that as the space decreases, the final population size decreases. At the same location (i.e., some fixed y), the pest population increased first and then decreased with the increase of dose time θ, occurring with hormetic effects. Similarly, for the fixed θ, the pest population desnity in different locations also showed some differences. The results shown in Fig. 16 and Fig. 17 all reveal that the occurrence of hormetic effects is spatially dependent. Due to the gradual decreasing of pesticide dose from the centre to the boundary area, different degrees of hormetic effects occur in the boundary area. The earlier the control is implemented or the smaller number of grids, the greater the intensity of the hormetic effects.

5. Conclusion and Discussion

In actual agricultural pest control, the spraying intensity of pesticides depends on the distribution of spatial areas. Typically, the central area of farmland is sprayed with high doses of pesticides, while in the surrounding areas the dosages gradually decrease. This inevitably leads to an increase in the dispersal rate of pest populations in farmland, posing a huge challenge for their control. Specifically, the spatiotemporal heterogeneity of pesticide dosage inevitably increases the possibility of hormetic effects such as low dose stimulation of pest population growth and high dose inhibition of its growth. Therefore, in order to reveal the effects of spatiotemporal heterogeneity, the intrinsic growth rate of the pest populations, pesticide efficiency and its application time on the complex dynamics, occurrence of hormesis in pest populations, we developed an integro-difference equation. This was based on the HRM and describes the associated complex dynamics and hormetic effects in two-dimensional space.

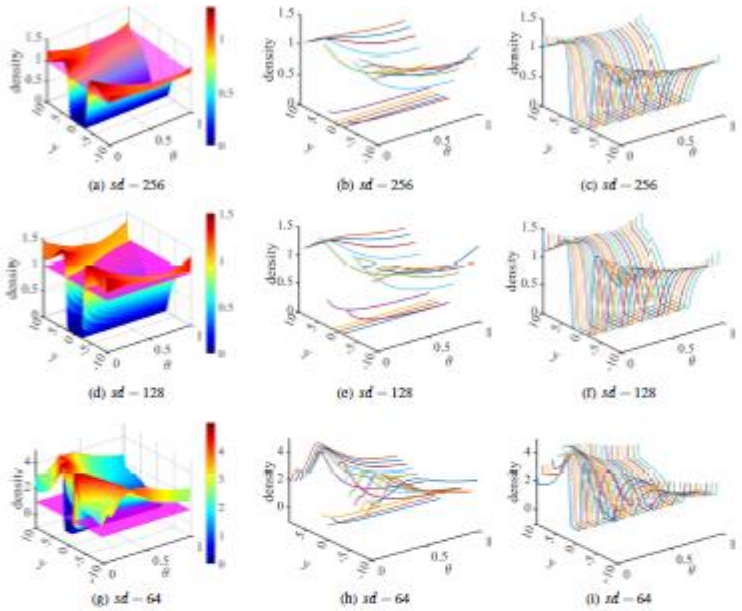

Figure 16: (y,θ)-dependence of the time-averaged population sizes over 100 generations for the model (2.13). (a,d,g): the steady-state solutions at a fixed observation position $(x^*,y(\cdot))$ with respect to θ for different sd; (b,e,h): the change curves with respect to θ under some fixed y; (c,f,i): the change curves with respect to y under some fixed θ. The other parameters are fixed as follows: $lx = 20, r = 1.9, K = 1, \mu = 0.02, T = 0.1$.

Our numerical analysis results are mainly reflected in two aspects. On the one hand, we investigate the effect of the intrinsic growth rate r, the application time θ and the application dose q on the population dynamics. As shown in Fig. 3(e) and Fig. 3(g), spraying insecticides does not completely reduce the pest population density, and only within a certain concentration can it inhibit pest increases. From Fig. 3 and Fig. 4 we can see that one parameter bifurcation analyses further reveal one of the most common features of hormesis: hormetic biphasic dose-responses (inverted U-shape or J-shape) of low dose stimulation and high-dose inhibition. An excessive intrinsic rate growth r will lead to the outbreak of the pest population, as shown in Fig. 5. The time of spraying insecticide θ has an effect on the pest population density, and

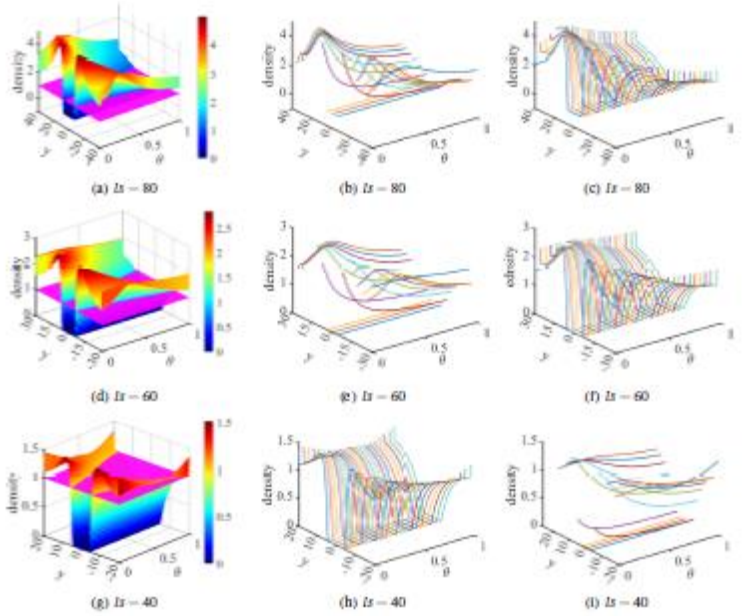

Figure 17: (y,θ)-dependence of the time-averaged population sizes over 100 generations for the model (2.13). (a,d,g): the steady-state solutions at a fixed observation position $(x^*, y(\cdot))$ with respect to θ for different sd; (b,e,h): the change curves with respect to θ under some fixed y; (c,f,i): the change curves with respect to y under some fixed θ. The other parameters are fixed as follows: $sd = 256, r = 1.9, K = 1, \mu = 0.02, T = 0.1$.

small values of θ will lead to increases of the pest population density (see Fig. 6). On the other hand, we reveal the impact of the characteristics of spatial regions including spatial grid and spatial domain on the dynamics of system. The numerical results were compared and analyzed under different values of sd or ls. The spatial grid sd and the spatial domain ls not only affect the dynamics of pests, but also are sensitive to the hormetic effects. As sd changes, the system appears multiple types of hormesis effect curves, and the stability of the system will also change. The conclusion is that the smaller the spatial grid sd, the smaller the parameter region where chaos occurs of the system, the stronger regeneration ability of the population. In addition, When the spatial grid sd is small, and the hormetic effect is more

obvious, as shown in Fig. 3. However, when the spatial grid sd reaches a certain threshold ($sd = 256$ in this paper), it has little effect on the population and hormetic effect. As ls increases, the number of pest population increase, the hormesis effect becomes more prominent curves, and the system stability becomes weaker.

If we want to control a pest population at a lower level than it was at the outset by spraying pesticides under the conditions modelled here, the smaller the spatial domain, the larger the amount of pesticides required (larger q) and the later is the optimal time for spraying pesticides (larger θ). At the same time, we can see from Fig. 9(a) and Fig. 9(b) that, under the current parameter space, the population size of the pest increased first and then decreased with the increasing of pesticide dose q when $\theta = 0.05$, and the density of the pest population increased in a large spatial domain ($ls = 80$ or $ls = 60$), (blue and red lines in Fig. 9(a)-Fig. 9(c)), it also shows a trend of increasing first and then decreasing with a fixed $q = 0.25$. Comparing Fig. 3(f) and Fig. 9(b), we can see that in the case of $ls = 40$ or $ls = 20$, and the amount of pesticide q required is also less, the pest population density can be well controlled, which can also reduce costs and ecological hazards. Therefore, another optimal role in determining the parameter space where hormetic effects occur is to avoid their occurrence and achieve successful or optimal pest control.

In Section 4.1 and Section 4.2, we consider spraying different concentrations of pesticides at different locations in space to enhance spatial heterogeneity, which makes the study further in line with practical applications. Understanding the mechanisms involved and the main factors influencing pest population growth will help to develop more effective pest control strategies and guide farmers to implement corresponding counter measures according to actual production conditions. All these results further confirm that optimal pest prevention and control measures not only rely on the efficiency of a pesticide and its application time, but also should be based on the spatial domain and with a reasonable grid, designed for effective prevention and control strategies while avoiding the occurrence of hormetic effects.

In this paper, we numerically investigated hormetic phenomena in an ecological population in two-dimensional space. The results obtained from numerical experiments show that the synergistic effect of multiple factors including killing rate q, dose time θ, spatial domain ls, spatial grid sd and other factors can significantly affect the dynamic behaviour and occurrence of hormetic effects. Thus we have provided insight into the system's complex dynamics and how to improve experimental designs and

analysis methods. The results presented here can be used to design and implement targeted pest control strategies to reduce unnecessary environmental damage, as well as providing a deeper understanding of the hormetic effects involved. However, there are many factors affecting the growth of pest populations, such as environmental temperature, natural enemies, resistance to pesticides and other external factors, which are also important for the process of integrated pest management. At the same time, our model has some shortcomings. For example, the diffusion of a population in space will be more complicated than as modelled here with the kernel function.

Appendix A. Proof of Theorem 3.1

Proof. It is easy to verify that a unique positive fixed point E^* arises when $pe^r > 1$. At E^*, the eigenvalue is $\lambda = -1$ if $C(N^*) = 0$.

In order to analyze the flip bifurcation around the fixed point $E^* = N^*$, we choose p as the bifurcation parameter and let $p = p_1$ as the critical value, which satisfies $C(N^*) = 0$ and $p_1 e^r > 1$. Let $u = N - N^*$ and $v = p - p_1$, where v is the new variable and is sufficiently small. We transform the fixed point E^* to the origin and expand the right-hand side of system (1.1) around the origin. Then system (1.1) becomes

$$\bar{F}(u,v) = A_1 u + A_2 v + A_3 u^2 + A_4 uv + A_5 v^2 + A_6 u^3 + A_7 u^2 v + A_8 uv^2 + A_9 v^2, \tag{A.1}$$

where

$A_1 = \frac{B_2 B_3 (rB_1 p_1 B_6 N^* + K) p_1}{K^2}$, $A_2 = \frac{B_2 (rB_1 B_6 p_1 N^* + K) N^*}{K}$,

$A_3 = \frac{p_1 B_2 r (p_1^2 r N^* B_1^2 B_3^2 B_5^2 + \left(B_4 \left(3r^2\theta^2 (N^*)^2 - 6Kr\theta N^* + 2K^2\right) p_1 B_1 - (2K - \theta N^* r)\theta K\right) K)}{2K^4}$,

$A_4 = \frac{B_2 B_3 \left((B_1 N^* p_1 B_4 r)^2 + 3B_1 K N^* p_1 B_6 r + K^2\right)}{K^3}$, $A_5 = \frac{B_1 B_2 B_6 r (N^*)^2 (rB_1 p_1 B_6 N^* + 2K)}{2K^2}$,

$A_6 = \frac{p_1 B_2 r^2 (B_1^2 r N^* (B_6 B_3 p_1)^3 + 3KB_3 (B_1 B_4 p_1 (K - 2(r\theta N^*)))^2 - K^2 B_6 B_1 \theta \left(7r^2\theta^2 (N^*)^2 - 21Kr\theta N^* + K^2\right) p_1 - K^3 r\theta^3 N^* + 3K^4\theta^2)}{6K^6}$,

$A_7 = \frac{B_2 r \left((rN^* B_3)^2 (B_1 B_4 p_1)^3 + Kr N^* (B_1 B_4 p_1)^2 \left(6(r\theta N^*)^2 - 12Kr\theta N^* + 5K^2\right) + K^2 \left(7(r\theta N^*)^2 - 14Kr\theta N^* + 7K^2\right) B_6 B_1 p_1 + K^3 r\theta^2 N^* - 2K^4\theta\right)}{2K^5}$,

$A_8 = \frac{N^* r B_1 B_2 B_3 B_6 (rN^* p_1 B_1 B_4 + 4K)(rN^* p_1 B_1 B_4 + K)}{2K^4}$ and $A_9 = \frac{(N^*)^3 B_2 (B_1 B_6 r)^2 (rN^* B_1 B_4 + 3K)}{6K^3}$.

After a simple calculation, we can get

$$\frac{\partial \bar{F}}{\partial u}(0,0) = A_1, \ \frac{\partial^2 \bar{F}}{\partial r \partial u}(0,0) = \frac{B_2 B_3 \left[(B_1 N^* p_1 B_6 r)^2 + 3B_1 K N^* p_1 B_6 r + K^2\right]}{K^3},$$

$$\frac{\partial^2 \bar{F}}{\partial u^2}(0,0) = \frac{p_1 B_2 r \left(rN^* (B_1 B_3 B_6 p_1)^2 + p_1 K B_1 B_4 \left(3(r\theta N^*)^2 - 6(r\theta N^*) + 2K^2\right) + K^2 r\theta^2 v - 2K^3\theta\right)}{K^4},$$

$\frac{\partial^3 F}{\partial u^3}(0,0) = \frac{p_1 B_2 r^2 (rN^*(B_1 B_2 B_4 p_1)^3 + 3KB_2(B_1 B_4 p_1)^2(2(rθN^*)^2 - 4Krθ N^* + K^2) - K^2 B_1 B_4 θ p_1 (7(rθN^*)^2 - 21Krθ z + 12K^2) - rN^* θ^3 K^3 + 3θ^2 K^4)}{K^6}$.

It is easy to verify that $\bar{F}'(0,0) = 0$, $\frac{\partial \bar{F}}{\partial u}(0,0) = -1$, $\frac{\partial^2 \bar{F}}{\partial \gamma \partial u}(0,0) \neq 0$, and $\frac{1}{2}\left(\frac{\partial^2 \bar{F}}{\partial u^2}(0,0)\right)^2 + \frac{1}{3}\frac{\partial^3 \bar{F}}{\partial u^3}(0,0) \neq 0$. By the theory of flip bifurcation in [56], if $pe^r > 1$ and $C(N^*) = 0$, a flip bifurcation occurs at E^*. The proof is completed. □

Appendix B. The calculation of Lyapunov exponent

First, we let

$$F_0(N) \doteq pN \exp\left[r\left(1 - \frac{N}{K}\left(\theta + (1-\theta)p\exp\left(r\left(1 - \frac{N}{K}\right)\theta\right)\right)\right)\right],$$

and denote $N_n = F_0^n(N_0) = F_0(F_0(\cdots(F_0(N_0))\cdots))$. Then we have

$$\left.\frac{\partial F_0^n}{\partial N}\right|_{N_0} = \left.\frac{\partial F_0'}{\partial N}\right|_{N_{n-1}} \cdot \left.\frac{\partial F_0'}{\partial N}\right|_{N_{n-2}} \cdots \left.\frac{\partial F_0'}{\partial N}\right|_{N_0}.$$

According to the formula for the Lyapunov exponents in [53], we can get the Lyapunov exponents of model (1.1), given by

$$\Lambda = \lim_{n\to\infty} \frac{1}{n}\sum_{i=0}^{n-1} \ln\left|\frac{dF_0(N_i,\phi)}{dN_i}\right|,$$

where ϕ is any parameter in the model (1.1). Discriminating the presence of chaotic motion in a nonlinear system involves checking whether its maximum Lyapunov exponential entry is positive [57]. The chaotic motion is identified as follows:

(1) when $\Lambda > 0$, the trajectory tends to a chaotic solution;

(2) when $\Lambda < 0$, the trajectory tends to a fixed point or periodic solution.

CRediT authorship contribution statement

Liwen Song: Conceptualization, Writing-original draft. Robert A. Cheke: Writing-review & editing. Changcheng Xiang: Visualization, Investigation. Sha He and Sanyi Tang: Methodology, Software, Funding acquisition, Writing-review & editing.

Declaration of Competing Interest

The authors declare no potential conflict of interests.

Acknowledgements

This work was supported by the National Natural Science Foundation of China (Grant No. 12031010, No. 12126350, No. 12201377 and No. 12361100).

Data availability

No data were used for the research described in the article.

References

[1] T D Luckey. Insecticide hormoligosis. *Journal of Economic Entomology*, 61(1):7–12, 02 1968.

[2] Joseph G Morse. Agricultural implications of pesticide-induced hormesis of insects and mites. *Human & Experimental Toxicology*, 17(5):266–269, 05 1998.

[3] Edward J Calabrese and Linda A Baldwin. Toxicology rethinks its central belief. *Nature*, 421(6924):691–692, 02 2003.

[4] Edward J Calabrese. Hormesis: changing view of the dose-response, a personal account of the history and current status. *Mutation Research/Reviews in Mutation Research*, 511(3):181–189, 07 2002.

[5] Jocelyn Kaiser. Sipping from a poisoned chalice. *Science*, 302:376–379, 10 2003.

[6] Nina Cedergreen, Jens C Streibig, Per Kudsk, Solvejg K Mathiassen, and Stephen O Duke. The occurrence of hormesis in plants and algae. *Dose-Response*, 5(2), 04 2007.

[7] Raul Narciso C Guedes, Rachel R Rix, and G Christopher Cutler. Pesticide-induced hormesis in arthropods: Towards biological systems. *Current Opinion in Toxicology*, 29:43–50, 02 2022.

[8] Evgenios Agathokleous, Giovanni Benelli, and Raul Narciso C Guedes. Plant-pest interactions under the microscope of chemical hormesis. *Trends in Plant Science*, 28(1):14–17, 10 2022.

[9] G Christopher Cutler, Marcel Amichot, Giovanni Benelli, Raul Narciso C Guedes, Yanyan Qu, Rachel R Rix, Farman Ullah, and Nicolas Desneux. Hormesis and insects: Effects and interactions in agroecosystems. *Science of The Total Environment*, 825:153899–153899, 02 2022.

[10] Kristina H Young, Jason R Baird, Talicia Savage, Benjamin Cottam, David Friedman, Shelly Bambina, David J Messenheimer, Bernard Fox, Pippa Newell, Keith S Bahjat, Michael J. Gough, and Marka R. Crittenden. Optimizing timing of immunotherapy improves control of tumors by hypofractionated radiation therapy. *PLOS ONE*, 11(6):e0157164, 06 2016.

[11] Raphael Serre, Sebastien Benzekry, Laetitia Padovani, Christophe Meille, Nicolas André, Joseph Ciccolini, Fabrice Barlesi, Xavier Muracciole, and Dominique Barbolosi. Mathematical modeling of cancer immunotherapy and its synergy with radiotherapy. *Cancer Research*, 76(17):4931–4940, 06 2016.

[12] Timothy W. Collins. Structural stability and morphogenesis: An outline of a general theory of models. *Contemporary Sociology*, 6(5):543–544, 09 1977.

[13] Karin E De Visser, Alexandra Eichten, and Lisa M Coussens. Paradoxical roles of the immune system during cancer development. *Nature Reviews Cancer*, 6(1):24–37, 01 2006.

[14] Flavio Salazar-Onfray, Mercedes N López, and Ariadna Mendoza-Naranjo. Paradoxical effects of cytokines in tumor immune surveillance and tumor immune escape. *Cytokine & Growth Factor Reviews*, 18(1-2):171–182, 02 2007.

[15] Zhiguang Li, Lin Chen, and Zhihai Qin. Paradoxical roles of il-4 in tumor immunity. *Cellular & Molecular Immunology*, 6(6):415–422, 12 2009.

[16] Oliver MT Pearce, Heinz Läubli, Jack Bui, and Ajit Varki. Hormesis in cancer immunology: Does the quantity of an immune reactant matter? *OncoImmunology*, 3(6):e29312, 06 2014.

[17] Jiuwei Cui, Guozi Yang, Zhenyu Pan, Yuguang Zhao, Xinyue Liang, Wei Li, and Lu Cai. Hormetic response to low-dose radiation: focus on the immune system and its clinical implications. *International Journal of Molecular Sciences*, 18(2):280, 01 2017.

[18] Andy Gaya, Charles A Akle, Satvinder Mudan, and John Grange. The concept of hormesis in cancer therapy–is less more? *Cureus*, 7(4), 04 2015.

[19] Qian Li and Yanni Xiao. Bifurcation analyses and hormetic effects of a discrete-time tumor model. *Applied Mathematics and Computation*, 363:124618, 12 2019.

[20] Oliver MT Pearce, Heinz Läubli, Andrea Verhagen, Patrick Secrest, Jiquan Zhang, Nissi M Varki, Paul R Crocker, Jack D Bui, and Ajit Varki. Inverse hormesis of cancer growth mediated by narrow ranges of tumor-directed antibodies. *Proceedings of the National Academy of Sciences*, 111(16):5998–6003, 04 2014.

[21] Edward J Calabrese, John W Staudenmayer, Edward J Stanek III, and George R Hoffmann. Hormesis outperforms threshold model in national cancer institute antitumor drug screening database. *Toxicological Sciences*, 94(2):368–378, 09 2006.

[22] Sandro Dattilo, Cesare Mancuso, Guido Koverech, Paola Di Mauro, Maria Laura Ontario, Cateno Concetto Petralia, Antonino Petralia, Luigi Maiolino, Agostino Serra, Edward J Calabrese, and Vittorio Calabrese. Heat shock proteins and hormesis in the diagnosis and treatment of neurodegenerative diseases. *Immunity & Ageing*, 12(1):1–19, 11 2015.

[23] Mehdi Nematbakhsh, Shaghayegh Haghjooyjavanmard, Farzaneh Mahmoodi, and Ali Reza Monajemi. The prevention of endothelial dysfunction through endothelial cell apoptosis inhibition in a hypercholesterolemic rabbit model: the effect of l-arginine supplementation. *Lipids in Health and Disease*, 7(1):1–6, 2008.

[24] Elena A Erofeeva. Hormesis and paradoxical effects of wheat seedling (triticum aestivum l.) parameters upon exposure to different pollutants in a wide range of doses. *Dose-Response*, 12(1):121–135, 07 2013.

[25] Ephraim Cohen. Pesticide-mediated homeostatic modulation in arthropods. *Pesticide Biochemistry and Physiology*, 85(1):21–27, 05 2006.

[26] Raul Narciso C Guedes and G Christopher Cutler. Insecticide-induced hormesis and arthropod pest management. *Pest Management Science*, 70(5):690–697, 12 2013.

[27] Tsutomu Matsuoka and Hiromi Seno. Ecological balance in the native population dynamics may cause the paradox of pest control with harvesting. *Journal of Theoretical Biology*, 252(1):87–97, 05 2008.

[28] Hiromi Seno. A paradox in discrete single species population dynamics with harvesting/thinning. *Mathematical Biosciences*, 214(1-2):63–69, 07 2008.

[29] Begoña Cid, Frank M Hilker, and Eduardo Liz. Harvest timing and its population dynamic consequences in a discrete single-species model. *Mathematical Biosciences*, 248:78–87, 02 2014.

[30] Yang Ni, Yan Meng, and Yiming Ding. Hopf bifurcation analysis for a modified time-delay predator-prey system with harvesting. *Journal of Applied Mathematics and Physics*, 03(7):771–780, 2015.

[31] Sanyi Tang and Robert A Cheke. State-dependent impulsive models of integrated pest management (ipm) strategies and their dynamic consequences. *Journal of Mathematical Biology*, 50:257–292, 10 2005.

[32] William Edwin Ricker. Stock and recruitment. *Journal of the Fisheries Research Board of Canada*, 11(5):559–623, 05 1954.

[33] G Carelli and I Iavicoli. Defining hormesis: the necessary tool to clarify experimentally the low dose–response relationship. *Human & Experimental Toxicology*, 21(2):103–104, 02 2002.

[34] Sanyi Tang, Juhua Liang, Changcheng Xiang, Yanni Xiao, Xia Wang, Jianhong Wu, Guoping Li, and Robert A Cheke. A general model of hormesis in biological systems and its application to pest management. *Journal of The Royal Society Interface*, 16(157):20190468, 08 2019.

[35] Bingtuan Li, Mark A Lewis, and Hans F Weinberger. Existence of traveling waves for integral recursions with nonmonotone growth functions. *Journal of Mathematical Biology*, 58(3):323–338, 09 2008.

[36] Bingtuan Li, Sharon Bewick, Michael R Barnard, and William F Fagan. Persistence and spreading speeds of integro-difference equations with an expanding or contracting habitat. *Bulletin of Mathematical Biology*, 78:1337–1379, 07 2016.

[37] Bingtuan Li and Jianhua Wu. Traveling waves in integro-difference equations with a shifting habitat. *Journal of Differential Equations*, 268(7):4059–4078, 03 2020.

[38] Bingtuan Li. Traveling wave solutions in a plant population model with a seed bank. *Journal of Mathematical Biology*, 65(5):855–873, 11 2012.

[39] Bingtuan Li. Multiple invasion speeds in a two-species integro-difference competition model. *Journal of Mathematical Biology*, 76(7):1975–2009, 01 2018.

[40] Ran Zhang and Shengqiang Liu. Traveling waves for svir epidemic model with nonlocal dispersal. *Mathematical Biosciences and Engineering*, 16(3):1654–1682, 2019.

[41] Ran Zhang, Jinliang Wang, and Shengqiang Liu. Traveling wave solutions for a class of discrete diffusive sir epidemic model. *Journal of Nonlinear Science*, 31:1–33, 01 2021.

[42] Ran Zhang and Xiaoqing Yu. Traveling waves for a four-compartment lattice epidemic system with exposed class and standard incidence. *Mathematical Methods in the Applied Sciences*, 45(1):113–136, 09 2021.

[43] Kai Wang, Hongyong Zhao, Hao Wang, and Ran Zhang. Traveling wave of a reaction-diffusion vector-borne disease model with nonlocal effects and distributed delay. *Journal of Dynamics and Differential Equations*, 45:1–37, 08 2021.

[44] Juhua Liang, Yaohua Zhu, Changcheng Xiang, and Sanyi Tang. Travelling waves and paradoxical effects in a discrete-time growth-dispersal model. *Applied Mathematical Modelling*, 59:132–146, 07 2018.

[45] Mark Andersen. Properties of some density-dependent integrodifference equation population models. *Mathematical Biosciences*, 104(1):135–157, 04 1991.

[46] Robert M May. Biological populations obeying difference equations: Stable points, stable cycles, and chaos. *Journal of Theoretical Biology*, 51(2):511–524, 06 1975.

[47] Robert M May. Simple mathematical models with very complicated dynamics. *Nature*, 261:459–467, 06 1976.

[48] Robert M May and George F Oster. Bifurcations and dynamic complexity in simple ecological models. *The American Naturalist*, 110(974):573–599, 07 1976.

[49] Jörg Waldvogel. The period in the volterra-lotka predator-prey model. *SIAM Journal on Numerical Analysis*, 20(6):1264–1272, 12 1983.

[50] Robert M Corless, Gaston H Gonnet, David EG Hare, David J Jeffrey, and Donald E Knuth. On the lambertw function. *Advances in Computational Mathematics*, 5:329–359, 12 1996.

[51] Mark Kot. Discrete-time travelling waves: Ecological examples. *Journal of Mathematical Biology*, 30:413–436, 02 1992.

[52] Mark Kot and William M Schaffer. Discrete-time growth-dispersal models. *Mathematical Biosciences*, 80(1):109–136, 07 1986.

[53] Thomas S Parker and Leon Chua. *Practical numerical algorithms for chaotic systems*. Springer Science & Business Media, 2012.

[54] S Neil Rasband. *Chaotic dynamics of nonlinear systems*. Courier Dover Publications, 2015.

[55] Marten Scheffer, Steve Carpenter, Jonathan A Foley, Carl Folke, and Brian Walker. Catastrophic shifts in ecosystems. *Nature*, 413(6856):591–596, 10 2001.

[56] Yuri A Kuznetsov, Iu A Kuznetsov, and Y Kuznetsov. *Elements of applied bifurcation theory*, volume 112. Springer, 1998.

[57] Sanyi Tang and Lansun Chen. Chaos in functional response host–parasitoid ecosystem models. *Chaos, Solitons & Fractals*, 13(4):875–884, 2002.